

# Electron-phonon superconductivity and charge density wave instability in the layered titanium-based pnictide $\text{BaTi}_2\text{Sb}_2\text{O}$

Alaska Subedi

Centre de Physique Théorique, École Polytechnique, CNRS, 91128 Palaiseau Cedex, France

(Dated: October 10, 2018)

I present the results of first principles calculations of the phonon dispersions and electron-phonon coupling for  $\text{BaTi}_2\text{Sb}_2\text{O}$ . The phonon dispersions show a weak lattice instability near the zone corners that leads to a charge-density wave phase. The calculations of the electron-phonon coupling reveal strong coupling, especially to the in-plane Ti modes. The total coupling is large enough to readily explain the superconductivity in this compound. As the Fermi surfaces are disconnected with different orbital character weights, this compound is likely to host a multiband superconductivity.

PACS numbers: 74.25.Kc, 74.20.Pq, 74.70.-b

## I. INTRODUCTION

The discovery of high-temperature superconductivity in iron based compounds by Kamihara *et al.*<sup>1</sup> has increased interest and intensified efforts to find superconductors in new families of compounds. These efforts have focused on searching for materials with structural, electronic and magnetic properties similar to those of the iron or cuprate superconductors. In particular, the ideal candidates are thought to be materials with a layered structure that are in proximity to a spin-density wave (SDW) instability due to Fermi surface nesting like in the iron based superconductors or a Mott insulating phase due to strong on-site Coulomb repulsion as in the cuprates.

Recently, Yajima *et al.* have reported superconductivity in  $\text{BaTi}_2\text{Sb}_2\text{O}$  with a  $T_c$  of 1.2 K.<sup>2</sup> Superconductivity in  $\text{Ba}_{1-x}\text{Na}_x\text{Ti}_2\text{Sb}_2\text{O}$  with a maximum  $T_c$  of 5.5 K has also been reported by Doan *et al.*<sup>3</sup> In addition to the superconducting transition, there is also an anomaly at  $T_a = 54$  K that manifests by showing strong features in the measurements of susceptibility, resistivity, and specific heat. The microscopic mechanism and the order parameter for this transition have not been determined but been ascribed to either a charge-density wave (CDW) or SDW instability. Furthermore, the superconducting phase coexists with this CDW or SDW phase.

This compound occurs in a tetragonal structure with space group  $P4/mmm$  and consists of square planes of transition element Ti. The O atoms are placed alternately at the center of the Ti squares such that each Ti atom has two O nearest neighbors. The Sb atoms are placed above and below the center of the Ti squares that do not contain O atoms. The  $\text{Ti}_2\text{Sb}_2\text{O}$  layers are stacked alternately with layers of Ba atoms along the  $c$  axis. This layered structure is similar to the iron based or cuprate superconductors as all of them have square planes of transition-metal atoms as a structural motif.

In addition, Singh has further highlighted similarities in the electronic and magnetic properties between  $\text{BaTi}_2\text{Sb}_2\text{O}$  and the iron superconductors based on first principles calculations.<sup>4</sup> The Fermi surface shows substantial nesting and leads to an antiferromagnetic insta-

bility as in the case of iron superconductors. This nested Fermi surface is consistent with the results of Pickett on a similar compound  $\text{Na}_2\text{Sb}_2\text{Ti}_2\text{O}$ , although he was unable to find a magnetically ordered state.<sup>5</sup> The electronic structure of  $\text{Na}_2\text{Ti}_2\text{Sb}_2\text{O}$  was also studied by de Biani *et al.* using tight-binding calculations, and they also find substantial nesting in the Fermi surface that may lead to a CDW instability.<sup>6</sup>

In any case, the presence of a nested Fermi surface and antiferromagnetic instability in  $\text{BaTi}_2\text{Sb}_2\text{O}$  leads Singh to predict a spin-fluctuation mediated superconductivity similar to that of the iron based superconductors.<sup>7</sup> The pairing state is predicted to have a sign-changing  $s$ -wave symmetry that is different from that of the iron based superconductors. Furthermore, spin fluctuations are repulsive in the singlet channel and hence are strongly pair-breaking for the attractive electron-phonon interaction. Thus, it is reasonable to expect that the superconductivity in  $\text{BaTi}_2\text{Sb}_2\text{O}$  is mediated by spin fluctuations, especially if the phase transition at  $T_a = 54$  K that coexists with the superconducting phase is due to SDW instability.

However, there are some differences between  $\text{BaTi}_2\text{Sb}_2\text{O}$  and other superconductors near magnetism. The maximum  $T_c = 5.5$  K of this compound is significantly smaller than that of the iron based or cuprate superconductors. This could be due to a small value of the Stoner parameter for Ti<sup>8</sup> or pair-breaking effects of the electron-phonon interaction. It is worthwhile to note that  $\text{Sr}_2\text{RuO}_4$ , which is purported to be an unconventional superconductor,<sup>9</sup> also has a small  $T_c$  of 1 K.<sup>10</sup> A more glaring difference is the very sensitive dependence of superconductivity on other constituent elements of the compound. A transition similar to the one in  $\text{BaTi}_2\text{Sb}_2\text{O}$  is also seen in other members of the family that includes  $\text{Na}_2\text{Ti}_2\text{Pn}_2\text{O}$  ( $\text{Pn} = \text{As}, \text{Sb}$ ),  $\text{BaTi}_2\text{As}_2\text{O}$ ,  $(\text{SrF})_2\text{Ti}_2\text{Pn}_2\text{O}$  ( $\text{Pn} = \text{As}, \text{Sb}$ ), and  $(\text{SmO})_2\text{Ti}_2\text{Sb}_2\text{O}$ ,<sup>11-19</sup> but superconductivity has so far only been observed in Na doped  $\text{BaTi}_2\text{Sb}_2\text{O}$ . This is in contrast to iron superconductors which exhibit superconductivity for a wide variety of cations and pnictogens. In the cuprates, superconductivity is also found for a wide variety of interlayer fillings that sepa-

rate the  $\text{CuO}_2$  layers. Even in the ruthenates, doping at the cation site or changing the interlayer spacing reveals various magnetic interactions. This suggests that the magnetism and mechanism for superconductivity in doped  $\text{BaTi}_2\text{Sb}_2\text{O}$  are quite different from those of other unconventional superconductors, and perhaps lattice instabilities and electron-phonon coupling play important roles.

In this paper, I present the results of first principles calculations that show presence of a CDW instability and a total electron-phonon coupling strong enough to yield a conventional superconductivity in  $\text{BaTi}_2\text{Sb}_2\text{O}$ . The phonon dispersions reveal a weak lattice instability near the Brillouin zone corners. This instability is associated with the elongation or compression of the Ti squares without an enclosed O such that the Ti squares with an O rotate either clockwise or counterclockwise by a small amount. I also find presence of strong electron-phonon couplings, especially near the zone corners. The total electron-phonon coupling  $\lambda_{\text{ep}} = 1.28$  for the undistorted structure or  $\lambda_{\text{ep}} = 0.55$  for the distorted structure is large enough to readily explain the superconductivity in this material.

## II. METHODS

The phonon dispersions and electron-phonon results presented here were obtained using density-functional perturbation theory<sup>20</sup> within the generalized gradient approximation of Perdew, Burke, and Ernzerhof<sup>21</sup> as implemented in the Quantum-ESPRESSO package.<sup>22</sup> I used the experimental lattice parameters ( $a = 4.11039 \text{ \AA}$  and  $c = 8.0864 \text{ \AA}$ )<sup>2</sup> but relaxed the internal Sb height parameter  $z_{\text{Sb}}$ . I obtained a value for  $z_{\text{Sb}} = 0.2493$ , which agrees well with both the experimental<sup>2,3</sup> and calculated<sup>4</sup> values. This is in contrast to the underestimation from density functional calculations found in the iron based superconductors.<sup>7</sup> This indicates that magnetism and/or lattice dynamics in  $\text{BaTi}_2\text{Sb}_2\text{O}$  might be different from those of the iron based superconductors.

I used pseudopotentials that were generated with the electronic configurations  $5s^25p^65d^06s^26p^0$ ,  $3s^23p^24s^23d^1$ ,  $5s^25p^35d^0$ , and  $2s^22p^43d^{-2}$ , respectively, for Ba, Ti, Sb, and O. In particular, it was necessary to include the semi-core states to get the electronic structure in close agreement with the results of the full-potential calculations. I used the cut-offs of 60 and 600 Ry for basis-set and charge density expansions, respectively. An  $8 \times 8 \times 4$   $\mathbf{k}$ -grid was used for the Brillouin zone integration during the self-consistency. For the undistorted structure, the dynamical matrices were calculated on an  $8 \times 8 \times 4$   $\mathbf{q}$ -grid, while the double-delta integration in the calculation of the electron-phonon spectral function was done on a  $24 \times 24 \times 12$  grid. For the distorted structure, I calculated the dynamical matrices on a  $4 \times 4 \times 4$   $\mathbf{q}$ -grid and used  $18 \times 18 \times 8$  grid for the double-delta integration. I used the generalized full-potential method as implemented in

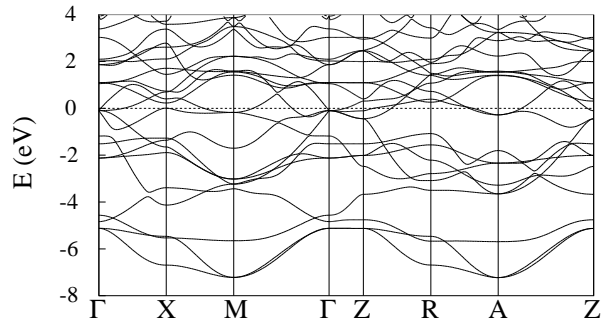


FIG. 1: Calculated GGA band structure of non-spin-polarized  $\text{BaTi}_2\text{Sb}_2\text{O}$  in the undistorted structure with experimental lattice parameters but relaxed internal coordinates.

the WIEN2k package<sup>23</sup> to perform the relaxation of the internal coordinates of a  $(\sqrt{2} \times \sqrt{2} \times 1)$  supercell. The muffin-tin radii of 2.4, 1.7, 2.4, and 1.7 Bohr were used for Ba, Ti, Sb, and O, respectively, and an  $8 \times 8 \times 8$   $\mathbf{k}$ -grid was used for the Brillouin zone integration.

## III. ELECTRONIC STRUCTURE

The electronic structure and magnetism of  $\text{BaTi}_2\text{Sb}_2\text{O}$  have been well described by Singh.<sup>4</sup> I summarize his results here for the sake of completeness. The band structure of this compound calculated using the pseudopotentials and plane-wave basis set is shown in Fig. 1. This agrees reasonably well with Singh's full-potential band structure that also includes the spin-orbit interaction. I also did full-potential band structure calculations without the spin-orbit coupling, and I find excellent agreement with the results from pseudopotential calculation. This shows that the pseudopotentials that I used are robust.

The three bands that lie between  $-7.3$  and  $-4.7$  eV have a dominant O  $2p$  character, and another six bands with mostly Sb  $5p$  character lie between  $-4.7$  and  $-0.5$  eV, relative to the Fermi energy. The bands near the Fermi level have mostly Ti  $3d$  character with some hybridization with Sb  $5p$  states, while the Ba  $6s$  states are above the Fermi level. This suggest that Ti ions are nominally trivalent and are in the  $d^1$  state, although the actual electron count will be different due to some covalency with O  $2p$  and Sb  $5p$  states.

The Fermi surface (not shown; see Ref. 4) has a very two dimensional, square electron sheet around zone corner  $M$  with mixed Ti  $d_{z^2}$ ,  $d_{x^2-y^2}$ , and  $d_{xy}$  characters. There is a three dimensional hole sheet around  $X$  with mostly Ti  $d_{z^2}$  with some admixture of  $d_{x^2-y^2}$  and  $d_{xy}$  characters. Around the zone center there is a complex three dimensional electron sheet with mixed  $d_{z^2}$  and  $d_{xy}$  character. In the calculations without spin-orbit coupling, there is also a small electron sheet around the zone center that has a mixed character. Singh calculated the

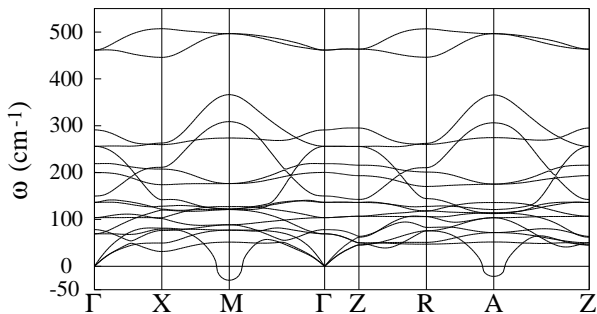


FIG. 2: Calculated GGA phonon dispersions of non-spin-polarized BaTi<sub>2</sub>Sb<sub>2</sub>O in the undistorted structure with experimental lattice parameters but relaxed internal coordinates. The imaginary frequencies are shown as negative.

real part of the susceptibility within the constant matrix element approximation and finds peaks in the susceptibility due to substantial nesting between Fermi sheets, especially near the  $\mathbf{q}$  vector  $(\frac{1}{2}, 0)$  ( $2\pi/a$ ). In addition, there is also a smaller peak near the  $\mathbf{q}$  vector  $(\frac{1}{2}, \frac{1}{2})$  ( $2\pi/a$ ). This could lead to magnetic instabilities at these  $\mathbf{q}$  vectors, although the height of the peaks could be diminished when the matrix element is explicitly taken into account in the calculation of the susceptibility. In any case, Singh finds that there is a magnetic instability at  $X$  that leads to a double stripe antiferromagnetic order with a doubling of the unit cell along either the  $a$  or  $b$  axis with small moments of  $0.2 \mu_B$  per Ti. Based on the proximity to the SDW instability, Singh predicts a spin-fluctuation mediated superconductivity in doped BaTi<sub>2</sub>Sb<sub>2</sub>O with a pairing state that has a sign-changing  $s$ -wave symmetry that is different from the one in the iron based superconductors.

#### IV. PHONONS AND ELECTRON-PHONON COUPLING

Although there seems to be a magnetic instability in BaTi<sub>2</sub>Sb<sub>2</sub>O, this does not preclude a competing lattice instability or an electron-phonon superconductivity. In this section, I show results that indicate that there is also a tendency to a CDW instability, although the energy of this state is higher than the SDW state obtained by Singh.<sup>4</sup> However, this CDW instability occurs at the wavevector  $(\frac{1}{2}, \frac{1}{2}, 0)$ , which is different from the wavevector  $(\frac{1}{2}, 0, 0)$  for the SDW instability. So, these two instabilities could coexist. Furthermore, I find that the electron-phonon coupling is large enough to readily explain the observed superconductivity.

The calculated phonon dispersions of BaTi<sub>2</sub>Sb<sub>2</sub>O in the undistorted tetragonal structure with the experimental lattice parameters and relaxed internal coordinates are shown in Fig. 2, and the corresponding phonon density of states along with atomwise projections are shown

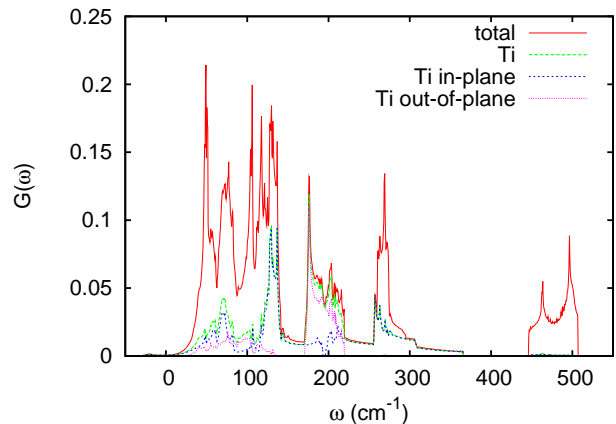
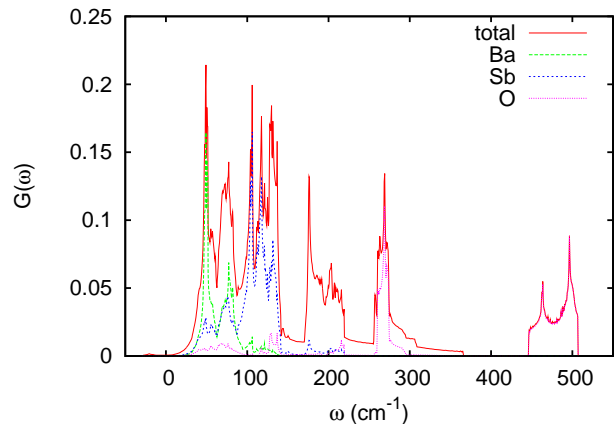


FIG. 3: (Color online) Top: Calculated GGA phonon density of states  $G(\omega)$  along with atomwise projections on Ba, Sb, and O of non-spin-polarized BaTi<sub>2</sub>Sb<sub>2</sub>O in the undistorted structure with experimental lattice parameters but relaxed internal coordinates. Bottom: Phonon density of states weighted by projections on Ti atom as well as its in-plane and out-of-plane characters.

in Fig. 3. A conspicuous feature of the phonon dispersions is the presence of an unstable mode around  $M$   $(\frac{1}{2}, \frac{1}{2}, 0)$  and  $A$   $(\frac{1}{2}, \frac{1}{2}, \frac{1}{2})$  indicating a CDW instability. The instability is weak with the maximum imaginary frequency of  $30i \text{ cm}^{-1}$ , suggesting a very shallow double well potential. The unstable mode has only in-plane Ti character, and the distortion corresponds to elongation or compression of the Ti squares without an enclosed O such that the Ti squares with O rotate either clockwise or counterclockwise by a small amount (see Fig. 4). I also performed relaxation of a  $(\sqrt{2} \times \sqrt{2} \times 1)$  super-cell with the full potential to check if the instability is a spurious effect of using pseudopotentials, and I again found a presence of this instability. The Ti ions get displaced by only  $0.096 \text{ \AA}$  from their original high-symmetry position. Although the Ti displacements are very small, I find a substantial reduction of the electronic density of states near the Fermi level with a reduction from a value

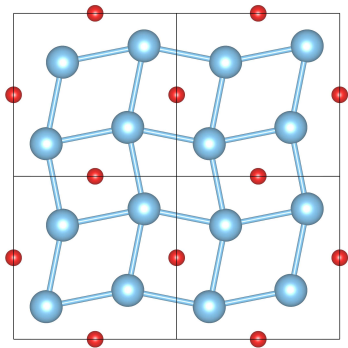


FIG. 4: (Color online) The distorted Ti plane in the CDW phase. The black grid shows the  $(\sqrt{2} \times \sqrt{2} \times 1)$  supercell relative to the undistorted structure. The big (cyan) balls represent Ti and small (red) balls are O. The Ti displacements are exaggerated to make the distortions conspicuous.

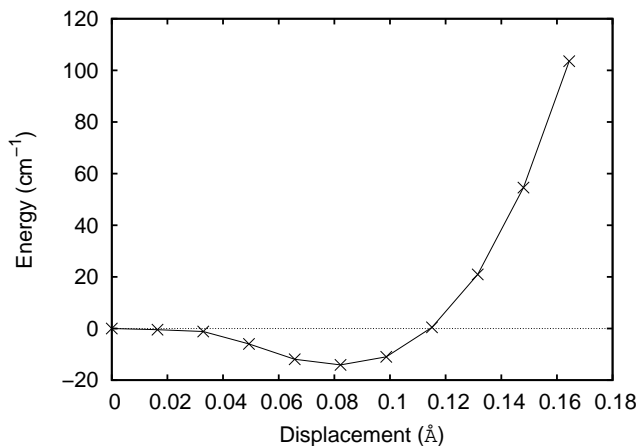


FIG. 5: Calculated anharmonic double-welled potential for the unstable mode obtained using frozen phonon method on a  $(\sqrt{2} \times \sqrt{2} \times 1)$  supercell. The energy is given per formula unit.

of  $3.88 \text{ eV}^{-1}$  per formula unit in the undistorted case to a value of  $2.83 \text{ eV}^{-1}$  per formula unit in the CDW phase, as obtained from full-potential calculations without spin-orbit coupling. In addition, I also performed frozen phonon calculations on the  $(\sqrt{2} \times \sqrt{2} \times 1)$  supercell by displacing Ti atoms according to the eigenvector of the unstable phonon mode. As shown in Fig. 5, the potential is anharmonic with a minimum at  $0.082 \text{ \AA}$ , and the depth of the well is very shallow at  $14.5 \text{ cm}^{-1}$ . Hence, it is not surprising that this CDW instability has so far been eluding detection.

Returning back to the phonon dispersions, the 18 modes of  $\text{BaTi}_2\text{Sb}_2\text{O}$  in the undistorted structure extend up to  $510 \text{ cm}^{-1}$ . There is a manifold of 16 bands with mixed Ba, Ti, Sb, and out-of-plane O character extending up to  $370 \text{ cm}^{-1}$ , which is separated by a gap from two in-plane O modes between  $445$  and  $510 \text{ cm}^{-1}$ . Within the lower manifold of 18 bands, the Ba vibrations

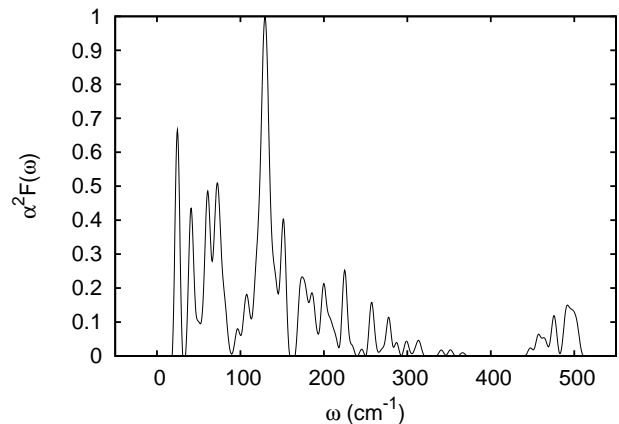


FIG. 6: Calculated Eliashberg spectral function of  $\text{BaTi}_2\text{Sb}_2\text{O}$  in the undistorted structure. The spectral weights for imaginary phonon frequencies are set to zero.

lie mostly within  $100 \text{ cm}^{-1}$ . The in-plane Ti character extends throughout this lower manifold, whereas the out-of-plane Ti modes are mainly confined to the two narrow bands within  $165$  and  $225 \text{ cm}^{-1}$ . Most of the Sb weight lies below  $145 \text{ cm}^{-1}$ , and the out-of-plane O modes lie between  $255$  and  $295 \text{ cm}^{-1}$ .

The strength of the interaction between electrons and phonons is generally given in terms of the Eliashberg spectral function,

$$\alpha^2 F(\omega) = \frac{1}{N(E_F)} \sum_{\mathbf{k}, \mathbf{q}, \nu, n, m} \delta(\epsilon_{\mathbf{k}}^n) \delta(\epsilon_{\mathbf{k}+\mathbf{q}}^m) |g_{\mathbf{k}, \mathbf{k}+\mathbf{q}}^{\nu, n, m}|^2 \delta(\omega - \omega_{\nu \mathbf{q}}), \quad (1)$$

where  $N(E_F)$  is the electronic density of states at the Fermi energy,  $\epsilon_{\mathbf{k}}^n$  is the electronic energy at wavevector  $\mathbf{k}$  and band index  $n$ ,  $\omega_{\nu \mathbf{q}}$  is the energy of a phonon with wavevector  $\mathbf{q}$  and branch index  $\nu$ , and  $|g_{\mathbf{k}, \mathbf{k}+\mathbf{q}}^{\nu, n, m}|^2$  is the matrix element for an electron in the state  $|n\mathbf{k}\rangle$  scattering to  $|m\mathbf{k} + \mathbf{q}\rangle$  through a phonon  $\omega_{\nu \mathbf{q}}$ . The calculated Eliashberg spectral function for  $\text{BaTi}_2\text{Sb}_2\text{O}$  is shown in Fig. 6. The spectral weight is spread through all the phonon frequencies, but it is specially enhanced at low frequencies below  $90 \text{ cm}^{-1}$  and between  $100$  and  $160 \text{ cm}^{-1}$ . I find that a substantial part of the spectral weight comes from modes that involve in-plane Ti vibrations. This is reasonable as the states near the Fermi level are dominated by Ti  $d$  character. Furthermore, the inter-layer Ti-Ti distance is much larger than the intra-layer Ti-Ti distance, and the coupling to the out-of-plane Ti modes is much smaller, as one might expect.

The  $\mathbf{q}$  dependent total electron-phonon coupling  $\lambda_{\mathbf{q}}$  ( $= \int_0^\infty d\omega \alpha^2 F(\omega, \mathbf{q}) / \omega$ ) is plotted for the  $k_z = 0$  plane of the Brillouin zone in Fig. 7. There are contributions to the electron-phonon coupling from throughout the Brillouin zone, but the magnitude of the electron-phonon coupling away from the zone center is much larger. In particular, the electron-phonon coupling is peaked near

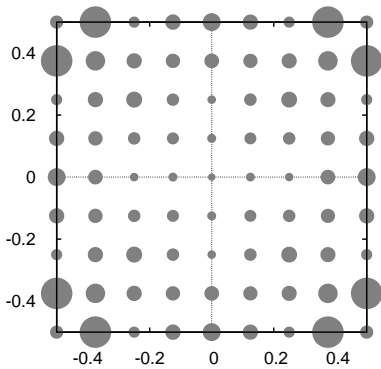


FIG. 7: Calculated  $\mathbf{q}$  dependent total electron-phonon coupling  $\lambda_{\mathbf{q}}$  shown for the  $k_z = 0$  plane of the Brillouin zone of the undistorted structure. The area of the circles is proportional to the magnitude of  $\lambda_{\mathbf{q}}$ . The unit of the axes is  $2\pi/a$ .

the wavevector  $(\pi/a, \pi/a)$ . Again, this is expected from the nesting between the Fermi sheets near the zone center and zone corners. Furthermore, since the disconnected Fermi sheets have different orbital character weights, the electron-phonon coupling on different Fermi sheets are likely to be different. Hence, this material is very likely to host a multiband superconductivity.

The total electron-phonon coupling constant is given by  $\lambda_{\text{ep}} = \sum_{\mathbf{q}, \nu} \lambda_{\mathbf{q}, \nu} = 2 \int_0^\infty d\omega \alpha^2 F(\omega) / \omega$ . For  $\text{BaTi}_2\text{Sb}_2\text{O}$ , I obtain  $\lambda_{\text{ep}} = 1.28$  with the logarithmically averaged frequency  $\omega_{\text{ln}} = 65 \text{ cm}^{-1}$ . (I obtain these numbers by setting the contribution from the imaginary frequencies to zero.) One can estimate the  $T_c$  within a single-band picture by inserting these numbers in the simplified Allen-Dynes formula,

$$T_c = \frac{\omega_{\text{ln}}}{1.2} \exp \left\{ -\frac{1.04(1 + \lambda_{\text{ep}})}{\lambda_{\text{ep}} - \mu^*(1 + 0.62\lambda_{\text{ep}})} \right\}.$$

With a value for the Coulomb pseudopotential parameter  $\mu^* = 0.1$ , I obtain  $T_c = 9.0 \text{ K}$ , which shows that the conventional electron-phonon picture readily explains the superconductivity in  $\text{BaTi}_2\text{Sb}_2\text{O}$ .

The above discussion of the phonon dispersions and the electron-phonon coupling concerned the undistorted structure, and it showed that there is both a CDW instability and a strong electron-phonon coupling that is large enough to yield superconductivity. However, it is more likely that the electron-phonon superconductivity occurs in the CDW phase, if it occurs at all. I performed calculations of the phonon dispersions and electron-phonon coupling for the distorted structure as well to check if the electron-phonon coupling is strong enough to give superconductivity.

The phonon dispersions and the Eliashberg spectral function for the distorted structure are shown in Figs. 8 and 9, respectively. As one expects, the phonon dispersions do not show any instabilities anymore showing that the distorted structure is dynamically stable. From

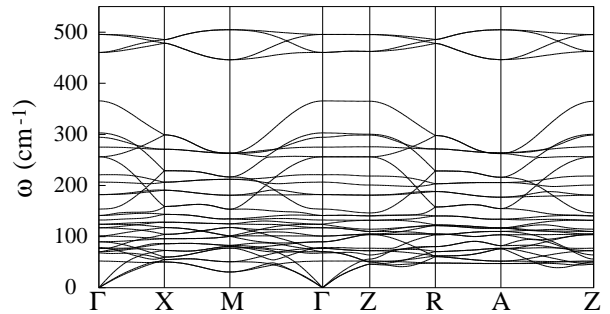


FIG. 8: Calculated GGA phonon dispersions of non-spin-polarized  $\text{BaTi}_2\text{Sb}_2\text{O}$  in the distorted structure.

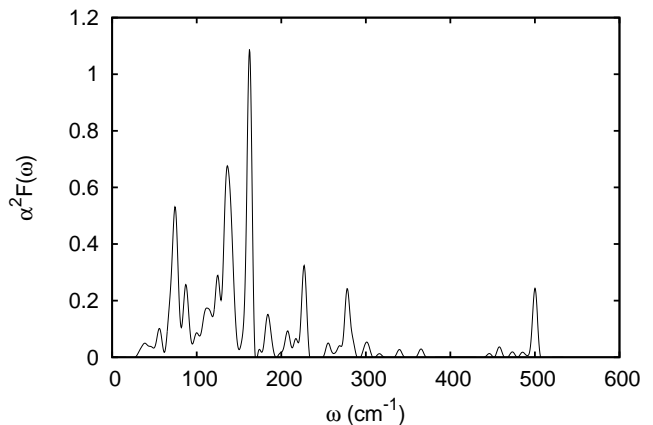


FIG. 9: Calculated Eliashberg spectral function of  $\text{BaTi}_2\text{Sb}_2\text{O}$  in the distorted structure.

Fig. 9, we see that the electron-phonon coupling to the modes below  $60 \text{ cm}^{-1}$  is greatly reduced as there is no contribution from the soft in-plane mode that existed in the undistorted structure. However, the coupling to the modes between  $60$  and  $170 \text{ cm}^{-1}$  remains significant.

In the distorted structure, I find for the total electron-phonon coupling a value of  $\lambda_{\text{ep}} = 0.55$  with the logarithmically averaged frequency  $\omega_{\text{ln}} = 110 \text{ cm}^{-1}$ . Using these values in the Allen-Dynes formula as above gives  $T_c = 2.7 \text{ K}$ , which is comparable to the experimentally obtained values of  $1.2$  and  $5.5 \text{ K}$ .<sup>2,3</sup>

## V. CONCLUSIONS

In summary, I have presented the results of phonon dispersions and electron-phonon coupling calculations for  $\text{BaTi}_2\text{Sb}_2\text{O}$ . The phonon dispersions show a weak lattice instability around Brillouin zone corners that gives rise to a CDW instability. The distortions correspond to elongation or compression of the Ti squares without an enclosed O such that the Ti squares with O rotate either clockwise or counterclockwise by a small amount. This results in a

( $\sqrt{2} \times \sqrt{2} \times 1$ ) doubling of the unit cell.

The electron-phonon calculations on the undistorted structure reveal the presence of strong electron-phonon couplings, especially to the in-plane Ti modes. There are contributions to the total coupling from throughout the Brillouin zone, but the magnitude of the couplings are large away from the zone center. The electron-phonon coupling is peaked near the zone corners at wavevectors that would correspond to the nesting vectors between the Fermi sheets around the zone center and zone corners. The total electron-phonon coupling is  $\lambda_{\text{ep}} = 1.28$ , which gives an estimate of  $T_c = 9.0$  K when inserted in the Allen-Dynes formula. The electron-phonon calcu-

lations on the distorted structure also show significant coupling with a value for the total electron coupling of  $\lambda_{\text{ep}} = 0.55$ . This gives an estimate of  $T_c = 2.7$  K for the distorted structure, which is in good agreement with the experimentally obtained values.

## VI. ACKNOWLEDGMENT

I gratefully acknowledge the use of the computer cluster of the Anderson department at Max Planck Institute, Stuttgart, Germany.

- 
- <sup>1</sup> Y. Kamihara, T. Watanabe, M. Hirano, and Hideo Hosono, *J. Am. Chem. Soc.* **130**, 3296 (2008).
- <sup>2</sup> T. Yajima, K. Nakano, F. Takeiri, T. Ono, Y. Hosokoshi, Y. Matsushita, J. Hester, Y. Kobayashi, and H. Kageyama, *J. Phys. Soc. Jpn.* **81**, 103706 (2012).
- <sup>3</sup> P. Doan, M. Gooch, Z. Tang, B. Lorenz, A. Möller, J. Tapp, P. C. W. Chu, and A. M. Guloy, *J. Am. Chem. Soc.* **134**, 16520 (2012).
- <sup>4</sup> D. J. Singh, *New J. Phys.* **14**, 123003, (2012).
- <sup>5</sup> W. E. Pickett, *Phys. Rev. B* **58**, 4335 (1998).
- <sup>6</sup> F. F. de Biani, P. Alemany, E. Canadell, *Inorg. Chem.* **37**, 5807 (1998).
- <sup>7</sup> I. I. Mazin, D. J. Singh, M. D. Johannes, and M. H. Du, *Phys. Rev. Lett.* **101**, 057003 (2008).
- <sup>8</sup> O. K. Andersen, O. Jepsen, and D. Glötzl, “Highlights of Condensed Matter Theory,” Eds. F. Bassani, F. Fumi, and M. P. Tosi (North-Holland, Amsterdam) 1985, p. 59.
- <sup>9</sup> T. M. Rice and M. Sigrist, *J. Phys. Condens. Matter* **7**, L643 (1995).
- <sup>10</sup> Y. Maeno, H. Hashimoto, K. Yoshida, S. Nishizaki, T. Fujita, J. G. Bednorz, and F. Lichtenberg, *Nature* **372**, 532 (1994).
- <sup>11</sup> A. Adam and H.-U. Schuster, *Z. Anorg. Allg. Chem* **584**, 150 (1990).
- <sup>12</sup> E. A. Axtell, III, T. Ozawa, S. M. Kauzlarich, and R. R. P. Singh, *J. Solid State Chem.* **134**, 423 (1997).
- <sup>13</sup> T. C. Ozawa, R. Pantoja, E. A. Axtell, III, S. M. Kauzlarich, J. E. Greedan, M. Bieringer, and J. W. Richardson, Jr., *J. Solid State Chem.* **153**, 275 (2000).
- <sup>14</sup> T. C. Ozawa, S. M. Kauzlarich, M. Bieringer, and J. E. Greedan, *Chem. Mater.*, **13**, 1804 (2001).
- <sup>15</sup> T. C. Ozawa and S. M. Kauzlarich, *J. Cryst. Growth* **256**, 571 (2004).
- <sup>16</sup> R. H. Liu, D. Tan, Y. A. Song, Q. J. Li, Y. J. Yan, J. J. Ying, Y. L. Xie, X. F. Wang, and X. H. Chen, *Phys. Rev. B* **80**, 144516 (2009).
- <sup>17</sup> X. F. Wang, Y. J. Yan, J. J. Ying, Q. J. Li, M. Zhang, N. Xu, X. H. Chen, *J. Phys.: Condens. Matter* **22**, 075702 (2010).
- <sup>18</sup> R. H. Liu, Y. A. Song, Q. J. Li, J. J. Ying, Y. J. Yan, Y. He, and X. H. Chen, *Chem. Mater.* **22**, 1503 (2010).
- <sup>19</sup> T. C. Ozawa and S. M. Kauzlarich, *Sci. Technol. Adv. Mater.* **9**, 033003 (2008).
- <sup>20</sup> S. Baroni, S. de Gironcoli, A. Dal Corso, and P. Giannozzi, *Rev. Mod. Phys.* **73**, 515 (2001).
- <sup>21</sup> J. P. Perdew, K. Burke, and M. Ernzerhof, *Phys. Rev. Lett.* **77**, 3865 (1996).
- <sup>22</sup> P. Giannozzi, S. Baroni, N. Bonini, M. Calandra, R. Car, C. Cavazzoni, D. Ceresoli, G. L. Chiarotti, M. Cococcioni, I. Dabo *et al.*, *J. Phys.: Condens. Matter* **21**, 395502 (2009).
- <sup>23</sup> P. Blaha, K. Schwarz, G. Madsen, D. Kvasnicka, and J. Luitz, “WIEN2k, An Augmented Plane Wave + Local Orbitals Program for Calculating Crystal Properties” (K. Schwarz, Tech. Univ. Wien, Austria) (2001).